Thermal Design of a Cryogenics Cooling System for a 10 MW-Class High-Temperature Superconducting Rotating Machine

Thanh Dung Le, *Student Member, IEEE*, Ji Hyung Kim, Sa Il Park, Dong-Hyung Kang, Haigun Lee, Young-Sik Jo, Yong Soo Yoon, and Ho Min Kim

***Abstract*—A cooling system is an essential part of high-temperature superconducting (HTS) rotating machine manufacturing. Moreover, thermal behavior is a crucial parameter of the cooling system that shows unique characteristics of superconductivity below a specific temperature to maintain a superconducting state. Therefore, many experiments have been performed to investigate new reliable cryogenic cooling systems for a large-scale HTS rotating machine. The motivation for the study is our recent development of the cryogenic cooling system using thermal trigger switches; it effectively minimizes non-operational downtime of the HTS machine in cases of power supply or cryocooler failure. This paper focuses on two main targets. First, the thermal design of the cooling system for the 10 MW-class HTS rotating machine is enhanced. Second, the performance of the cooling system is observed for various cryogens to investigate the feasibility of using solid cryogen.**

***Index Terms*—Cryogenics cooling system, current leads, high Tc superconducting (HTS) generator, thermal characteristics.**

I. Introduction

SEVERAL POWER utility applications designs have been based on the exploitation of the high temperature superconductor discovery in 1986 by Muller and Bednorz [1], mainly because the cooling systems are easily and reasonably cooled with liquid nitrogen at considerably higher temperatures. Moreover, the high temperature superconductor material can permit higher magnetic flux and a unique higher current-carrying capability than that of low temperature (LTS), so HTS rotating machines provide the highest power density when compared with conventional ones. Because of the significant increase in both electrical and magnetic loading, they are smaller and lighter in structure [2] and have less energy consumption, leading to a reduced energy cost [3].

The advantage of using the Gifford-McMahon (G-M) cryocooler in superconducting wind generators is not only their small size and simple operation, as illustrated in [4], but also their high reliability. In consideration of these advantages and rapid developments in the HTS rotating machine (according to the added complexity of keeping the field winding at 30 K), it is extremely necessary to parallel reinforce the cryogenic cooling system reliability, and effectiveness. Consequently, we have proposed a recent study optimizing design specifications for a 10 MW-class HTS synchronous generator wind power [5], [6] and comparative analysis of the cryogenic cooling device prototype performance [7]. This study continues to analyze thermal characteristics of cooling system to diminish thermal absorption from room temperature whenever the cryocooler fails; hence, it will optimize total volume of solid cryogens to remain in the HTS field coils, which are kept in a cryostat, and are kept below a certain temperature as long as desired.

II. Configuration of Cooling Method

According to recent studies [8], a solid cryogen, which has a large heat capacity, enables the HTS magnet systems to take advantages of the HTS magnet's ability. It capably maintains a constant field over a wide operating range. Particularly, having a large enthalpy with a minimal weight of the cold body of solid cryogen can enable the HTS magnet system to be compact and portable by increasing the recooling-to-recooling time period (RRTP) value. Therefore, this study explored the feasibility of a cooling system using a solid cryogen as a cryogen for the 10 MW-class HTS synchronous generator. Fig. 1 depicts the configuration of the solid cryogen cooling system, including significant components: a two-stage cryocooler, a solid cryogen tank, a thermal trigger switch, and a basic schematic view of a HTS rotating machine conceptual design. Its operation will be clearly explained hereafter.

III. Total Thermal Loss Estimation

The total heat loss of the cryogenic cooling system can be expressed conveniently as:

$$Q_{total} = Q_k + Q_{conv} + Q_{rotor}. \quad (1)$$

Manuscript received August 9, 2014; accepted January 20, 2015. Date of publication January 23, 2015; date of current version March 13, 2015. This work was supported by the International Collaborative R&D Program and the New and Renewable Energy of the Korea Institute of Energy Technology Evaluation and Planning (KETEP) grant funded by the Korea Government Ministry of Knowledge Economy (No. 20118520020020 and 20113020020020).

T. D. Le, J. H. Kim, S. I. Park, and H. M. Kim are with the Electrical Engineering Department, Jeju National University, Jeju-si 690-756, Korea (e-mail: ltdung@ctuet.edu.vn; hmkim@jejunu.ac.kr).

D.-H. Kang and H. G. Lee are with the Department of Materials Science and Engineering, Korea University, Seoul 136-701, Korea (e-mail: haigunlee@korea.ac.kr).

Y.-S. Jo is with the Korea Electrotechnology Research Institute, Changwon-si 642-120, Korea (e-mail: ysjo@keri.re.kr).

Y. S. Yoon is with the Department of Electrical Engineering, Shin Ansan University, Ansan-si 425-792, Korea (e-mail: ysyoon@sau.ac.kr).

Color versions of one or more of the figures in this paper are available online at http://ieeexplore.ieee.org.

Digital Object Identifier 10.1109/TASC.2015.2395721

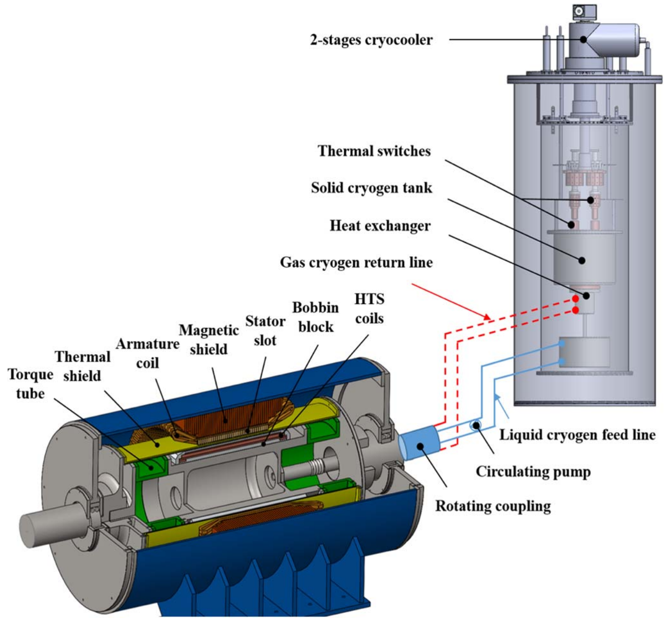

Fig. 1. Configuration of the cooling system, and basic schematic view of the HTS rotating machine conceptual design.

There are two main losses in the cooling system. First is conduction loss Q_k, which describes the heat loss through support rods and copper thermal switch pillars. Natural convection Q_{conv} is the proposed relationship describing heat loss when a heat sink-cooled surface is exposed directly to ambient air flow of Helium has on a heat exchanger. The inside heat loss Q_{rotor}, accounts for 1) conduction loss via current lead, torque tube, and residual gas, 2) radiation loss, and 3) superconducting coil losses including Joule heating loss at mechanical lap joints, eddy current loss, and Joule heating loss in terms of intrinsic property n-value. In certain assumptions, the HTS winding temperature and the inner pressure in the cryostat are at 30 K and at 10^{-5} torr (1.33 MPa), respectively. Then, the total heat loss of the rotor is evaluated as follows:

A. Current Lead Loss

For a conduction-cooled metal lead operating between room temperature and cold-end temperature, the steady state lead power differential equation over a unit lead length according to variable diameter has been derived an approximate equation [9]

$$Q_c = \left(k(T)A\frac{dT}{dz} + \rho(T)I^2\frac{dTdz}{A} \right)\Bigg|_{z=l} \tag{2}$$

where T and A are the temperature and the cross-section at $z = l$, respectively, while $k(T)$ and $\rho(T)$ are the thermal conductivity and electrical resistivity of material at T temperature, and I is the system operating current. Q_c is the total heat loss at the cold end for each part of the lead. Consequently, the optimal design copper current lead with the optimum loss was estimated 34.34 W for one pair of leads.

B. Conduction Heat Loss of the Torque Tube

Most heat invasion originates from heat conduction along the main rotor shaft. G-10 material is used to design the torque tube because of its low thermal conductivity ($k = 0.53$ W/m.K). Considering the mechanical strength of G-10 material, the designed transmission torque was 9554.14 kNm (10 MW, at 10 rpm, direct driven, 24 poles) [5]. The conduction heat leak of the torque tube can be calculated as follows:

$$Q_t = \frac{kA}{\delta}\Delta T \tag{3}$$

where Q_t is the conduction heat leak of the torque tube, k is the thermal conductivity of the material which is dependent on temperature. ΔT, δ, A are the temperature difference, the length of the torque tube and the equivalent cross-sectional area, respectively. Fig. 2 highlights the relative relationship of torque tube conduction loss on the inner diameter and torsion angle σ. For safety, the torsion angle σ must be within 0.2–0.3°. The optimal inner diameter was selected at 3.21 m because of less conduction heat loss and a safer conditions. The stress analysis and heat loss characteristics of the torque tube is summarized in Table I for various length tubes.

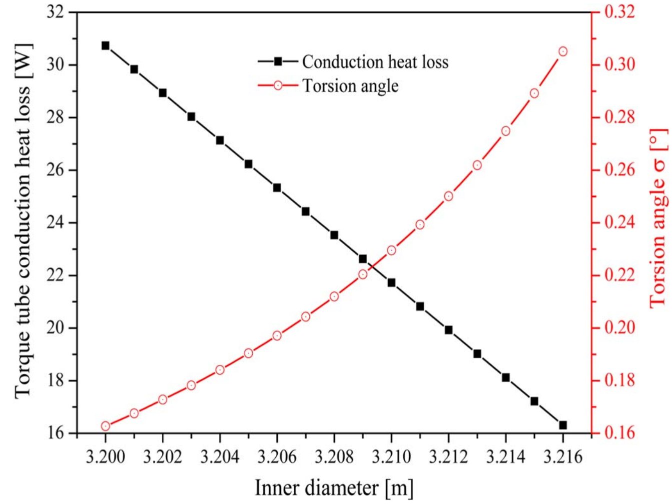

Fig. 2. Relative relationship between torque tube conduction loss, torsion angle and the inner diameter (at 0.8 m torque tube length).

TABLE I
STRESS ANALYSIS AND HEAT LOSS OF G-10 TORQUE TUBE

	Case I	Case II	Case III	Case IV
Length [m]	0.40	0.60	0.80	1.0
Outer diameter D_{out} [mm]	3234	3234	3234	3234
Inner diameter D_{in} [mm]	3210	3210	3210	3210
Young's modulus [GPa]	18	18	18	18
Yield strength [MPa]	280	280	280	280
Poison ratio	0.19	0.19	0.19	0.19
Maximum shear stress [MPa]	49.03	49.03	49.03	49.03
Conduction heat loss [W]	86.90	57.94	43.45	34.76

C. Radiation Heat Loss

A significant decrease in radiation heat loss can be achieved by wrapping the HTS coil with superinsulation layers. Radiation loss between the enclosure and the thermal shield with

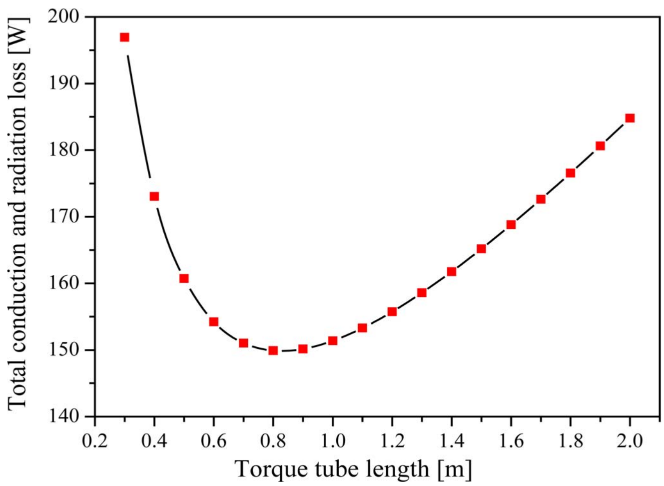

Fig. 3. Interdependence of torque tube length and radiation heat loss.

the presence of superinsulation layers number N_i is estimated as [10]:

$$Q_r = \frac{\varepsilon\sigma}{N_i + 1}\left(T_w^4 - T_c^4\right) \tag{4}$$

where ε is the effective total thermal emissivity of the materials, and σ is Stefan-Boltzmann constant. T_w and T_c are the enclosure temperature and thermal shield temperature, respectively. As noted from [10], the largest radiative heat flux $Q_r = 2.5$ W/m^2 (with 60 superinsulation layers). Then, radiation loss relies on radiation area S, which can be calculated by the rotor's dimensions.

Torque tube conduction loss is conversely proportional to torque tube length. In contrast, whenever torque tube length is increased, it will surely lead to radiation area S increases. As a result, radiation loss will linearly escalate. Subsequently, the optimal radiation loss is 106.45 W, where torque tube length is 0.8 m, as shown in Fig. 3.

D. Residual Gas Conduction Loss

The residual gas, which mostly accounts for the outgassed surface of cryostat structural components, metals, and nonmetals, will be conducted, and the conduction heat loss of residual gas can be approximately given by [10]:

$$Q_g = \eta_g P_g S \Delta T \tag{5}$$

where the accommodation coefficient η_g depends on the warm temperature T_{wm} and the cold temperature T_{cl}. P_g is the pressure of the gas in the Dewar. ΔT, S are the different temperatures between the first thermal shield and the high temperature superconducting coils, and the cross-section facing the radiation shields, respectively.

E. Superconducting Coils Loss

1) Joule Heating Loss at Mechanical Lap Joints: It is unavoidable to make joints in the tape length because of the limited availability of tape lengths from manufacturers. Total

TABLE II
THERMAL LOSS ESTIMATION

Quantity	Value [W]
Total loss	233
Conduction via rods & convection via heat exchanger	9.33
Current leads conduction loss	34.35
Torque tube conduction loss	43.45
Radiation loss	106.45
Residual gas conduction	9.79
Lap joints Joule heating loss	9.29
Eddy current loss and index loss	20.33

joint resistance is conveniently estimated as 0.05 $\mu\Omega$ [11]. Consequently, Ohmic Joule heat loss can be calculated.

$$Q_j = N_j I^2 R_j \tag{6}$$

where Q_j, I, R_j, N_j are the Joule heating loss, operating current, total joint resistance, and total number of mechanical lap joint of HTS tapes, respectively. The total HTS wire length is 1036 km at its highest efficiency, 96.71% [6]. Then, the N_j is 3453 joints where the routinely manufacturing long single-piece HTS length is 100–300 m. Therefore, Q_j is estimated 9.29 W.

2) Eddy Current Loss: Another loss that must be handled is the eddy current loss. The formula for its energy density e_{ed} in the low frequency limit for a tape is indicated as follows [10]:

$$e_{ed} = \frac{4\pi^2(\mu_0 \lambda H_m)^2}{24\rho_m \tau_m}. \tag{7}$$

3) Index Loss: Index loss depends on the intrinsic n-value HTS materials. It is necessary to consider the index voltage only in the maximum field region. By integrating the E field over a conductor length l_{mx} we can see that the resistive voltage causes a current decay in the magnet of inductance L_m with operation current I_{op} and critical current I_c. That can be expressed as Equation (8) [10]:

$$\frac{dI_{op}}{dt} = -\frac{E_c}{L_{m\,c}}\left(\frac{I_{op}}{I_c}\right)^n l_{mx}. \tag{8}$$

A detailed summary of each heat loss of cooling system for the 10 MW-class HTS synchronous generator is listed in Table II, where eddy current loss and index loss is estimated equal to 1% of the total loss. Correspondingly, the total estimation heat loss, or Q_{total}, is 233 W. It is comparable to the thermal load estimation of 12 MW direct-drive superconducting synchronous wind generator at 40 K, which was recently announced [12], [13].

IV. CRYOGENICS COOLING SYSTEM DESIGN

Fig. 4 presents the primary components that comprise the prototype of the cryogenic cooling system. The system can be classified into four main parts: a cold head, a thermal trigger switch, a cryogen tank and a heat exchanger with thermo-syphon technique. In addition, the detailed schematic of the solid cryogen tank, which is the main cooling source

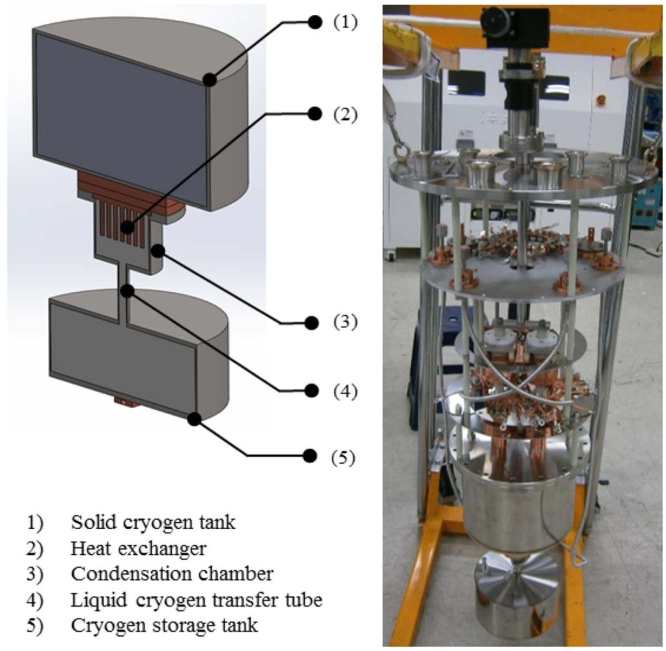

Fig. 4. Schematic of a 3D drawing model of solid cryogen cooling system via copper heat exchanger (left), and prototype of cooling device for superconducting rotating machines using a thermal trigger switch (right).

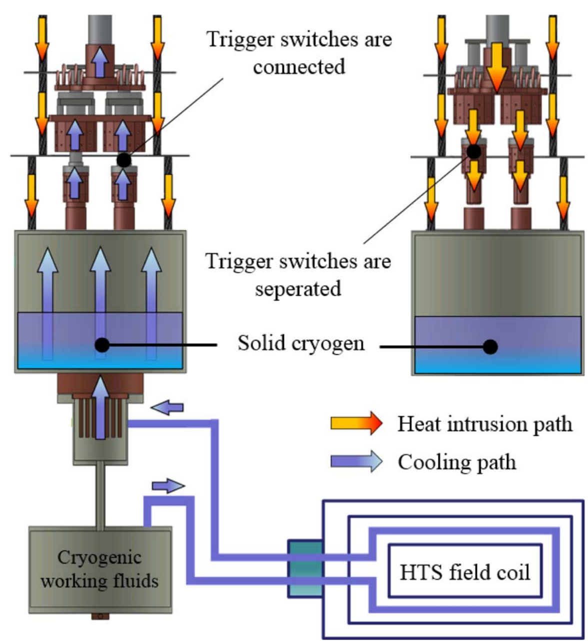

Fig. 5. The principle operation of a cooling system using thermal trigger switches at normal operation (left), and thermal trigger operating switches (right).

based on conduction method via copper heat exchanger, is also illustrated.

The device's principle application is to eliminate parasitic heat loss. As shown in Fig. 5, in case of normal operations, cryogen for cooling HTS field coils is made through the cryocooler. However, whenever the failure of the cryocooler occurs because of heat intrusion increases from room temperature, the cooling load is rapidly increased. To minimize the heat intrusion from room temperature, a trigger switch disconnects the thermal trigger switch and the thermal trigger switch socket.

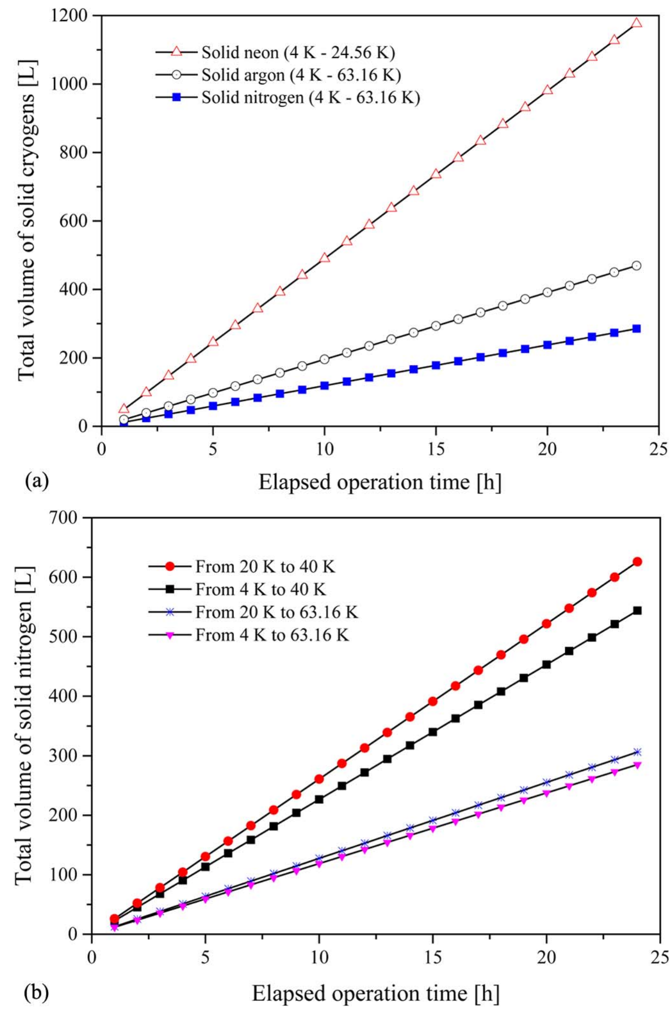

Fig. 6. The various calculated values of (a) total volume different solid cryogens versus Δt (b) the total volume of solid nitrogen varying on Δt and different initial temperatures and the final temperature range.

The duration for the system to remain detached from its cooling source is arbitrarily selected as 24 h. Then, to create an optimal design of a solid cryogen cooling system, it is essential to obtain the total volume of solid cryogen vessel. The total volume of the solid cryogen vessel V_{sc} is determined by the following equation [14]:

$$V_{sc} = \frac{Q_{total}}{\Delta H}\Delta t \tag{9}$$

where Q_{total} is the total heat loss of the cooling system, and Δt is the duration of the temperature variation of solid cryogen from the initial temperature (T_i) to the final temperature (T_f). The total enthalpy change of solid cryogen ΔH is expressed as:

$$\Delta H = \int_{T_i}^{T_f} C_p(T)dT \tag{10}$$

where C_p is the specific heat of the solid cryogen, which is highly dependent on the temperature of the materials.

A number of factors were carefully considered when selecting nitrogen as the optimum cryogen to use for this cryogenic system. First, the cost is less expensive in comparison to other cryogens because of its availability. Second, it has a higher specific heat capacity (per unit mass) than other common cryogens such as neon and argon. Third, the latent heat of solid nitrogen goes through a solid-solid phase transition at 35.6 K, increasing solid cryogen's ability to absorb heat although liquid nitrogen freezes at 63.2 K. Thus, it can initially be cooled below this point [15]. Within a 24 h duration and a total heat loss (Q_{total}) of 233 W, the volume of solid nitrogen as a solid cryogen (285 L) is about 65% less than solid argon (469 L) and over four times smaller than solid neon (1,176 L), as shown in Fig. 6.

Moreover, Fig. 6 also illustrates the total volume of solid cryogens according to different temperature ranges. A wider range of temperature will lead to smaller amounts of cryogen volumes used. Solid nitrogen from 63.16 K to 20 K is much more effective than the 4 K level because the difference total volume is insignificant, just 21 L, while the cooling process cost and difficulty requires much effort. It was then decided that the solid cryogen should be cooled to 20 K using a two-stage cryocooler, and the magnet should be operated between $T_i = 20$ K and $T_f = 63.16$ K (below the freezing point of nitrogen).

V. Conclusion

High performance, reliability, and optimal cooling systems are characterized in this study. The device's principle application is to eliminate parasitic heat loss from systems' non-operating cryocoolers. Therefore, it can utilize cryocooler redundancy and downplay the cryogen usage in Dewar systems. Because of the significant savings in refrigeration power, cryogen consumption can be achieved with a short investment return time period and at a relatively low cost.

In cases of cryocooler failures, it is estimated that 306 L of solid nitrogen is used to keep the cryostat, whose total optimum heat leak is 233 W, constantly operated within a 24 h period between 20 K and 63.16 K.

References

[1] K. A. Muller and J. G. Bednorz, "The discovery of a class of high-temperature superconductors," *Science*, vol. 237, no. 4819, pp. 1133–1139, Sep. 1987.

[2] D. Zhou *et al.*, "An overview of rotating machine systems with high temperature bulk superconductors," *Supercond. Sci. Technol.*, vol. 25, no. 10, Oct. 2012, Art. ID. 103001.

[3] W. Tong, *Wind Power Generation and Wind Turbine Design*. Southampton, U.K.: WIT Press, 2010.

[4] G. Snitchler, B. Gamble, C. King, and P. Winn , "10 MW class superconductor wind turbine generators," *IEEE Trans. Appl. Supercond.*, vol. 21, no. 3, pp. 1089–1092, Jun. 2011.

[5] J. H. Kim and H. M. Kim, "Electromagnetic design of 10 MW-class superconducting wind turbine using 2G HTS wire," *Progr. Supercond. Cryogenics*, vol. 15, no. 3, pp. 29–34, 2013.

[6] J. H. Kim, S. I. Park, T. D. Le, and H. M. Kim, "3D electromagnetic design and electrical characteristic analysis of a 10-MW-class high temperature superconducting synchronous generator for wind power," *Progr. Supercond. Cryogenics*, vol. 16, no. 2, pp. 47–53, Jun. 2014.

[7] S. H. Im *et al.*, "Performance test of a cryogenic system for superconducting rotating machines using the thermal trigger switch," presented at the 23rd Int. Conf. Magnet Technol., Boston, MA, USA, Jul. 2013, Paper 3PoAC-09.

[8] B. J. Haid *et al.*, "A 'permanent' high-temperature superconducting magnet operated in thermal communication with a mass of solid nitrogen," *Cryogenics*, vol. 42, no. 3/4, pp. 229–244, Mar. 2002.

[9] T. D. Le, J. H. Kim, S. I. Park, and H. M. Kim, "Conceptual design of current lead for large scale high temperature superconducting rotating machine," *Progr. Supercond. Cryogenics*, vol. 16, no. 2, pp. 54–58, 2014.

[10] Y. Iwasa, *Case Studies in Superconducting Magnets: Design and Operational Issues*, 2nd ed. New York, NY, USA: Springer-Verlag, 2009, pp. 248–252, 400–443, 457–458.

[11] Y. Senio, S. Ito, and H. Hashizume, "Joint resistance characteristics of mechanical lap joint of a GdBCO tape with a change in temperature and magnetic field," *IEEE Trans. Appl. Supercond.*, vol. 24, no. 3, Jun. 2014, Art. ID. 4602105.

[12] Z. Zhu, R. Qu, and J. Wang, "Conceptual design of the cryostat for a direct-drive superconducting wind generator," *IEEE Trans. Appl. Supercond.*, vol. 24, no. 3, Jun. 2014, Art. ID. 5201304.

[13] J. He *et al.*, "Conceptual design of the cryogenic system for a 12 MW superconducting wind turbine generator," *IEEE Trans. Appl. Supercond.*, vol. 24, no. 3, Jun. 2014, Art. ID. 5201105.

[14] B. J. Haid *et al.*, "Design analysis of a nitrogen cooled permanent high-temperature superconducting magnet system," *Cryogenics*, vol. 42, no. 10, pp. 617–634, Oct. 2002.

[15] P. Hales, H. Jones, S. Milward, S. Harrison, "Investigation into the use of solid nitrogen to create a 'thermal battery' for cooling a portable high-temperature superconducting magnet," *Cryogenics*, vol. 45, no. 2, pp. 109–115, Feb. 2005.